ACS APPLIED NANO MATERIALS
Cite This: ACS Appl. Nano Mater. XXXX, XXX, XXX−XXX
Article
www.acsanm.org

A Mesoporous Aluminosilicate Nanoparticle-Supported Nickel−Boron Composite for the Catalytic Reduction of Nitroarenes

Jesse L. Hauser,[†] Gabriella Amberchan,[†] Monique Tso,[†] Ryan Manley,[†] Karen Bustillo,[‡] Jason Cooper,[§] Josh H. Golden,[†] Bakthan Singaram,*[,†] and Scott R. J. Oliver*[,†]

[†]Department of Chemistry and Biochemistry, University of California, Santa Cruz, Santa Cruz, California 95064, United States
[‡]National Center for Electron Microscopy, Molecular Foundry, and [§]Chemical Sciences Division, Lawrence Berkeley National Laboratory, Berkeley, California 94720, United States

Supporting Information

ABSTRACT: An amorphous nickel and boron composite (NBC) was synthesized from nickel chloride hexahydrate ($NiCl_2·6H_2O$) and sodium borohydride ($NaBH_4$) in absolute ethanol, both in bulk and supported on mesoporous aluminosilicate nanoparticles (MASN). Comparatively, NBC-MASN demonstrated better catalytic activity for the selective reduction of the nitro group on a variety of polysubstituted nitroarenes, using hydrazine hydrate ($N_2H_4·H_2O$) as the reducing agent at 25 °C. Reuse and regeneration of NBC-MASN for the reduction of *p*-nitrotoluene to *p*-toluidine were studied with $NaBH_4$ acting as a regeneration agent. Good catalytic activity was sustained through nine reuse cycles when equimolar $NaBH_4$ was present in situ with $N_2H_4·H_2O$ (99%−67% isolated aniline yield). The structure and composition of NBC and NBC-MASN were examined by electron microscopy, energy dispersive X-ray spectroscopy (EDS), powder X-ray diffraction (PXRD), X-ray photoelectron spectroscopy (XPS), thermogravimetric analysis (TGA), and inductively coupled plasma optical emission spectroscopy (ICP-OES). The results for NBC-MASN show that a thin (<10 nm) amorphous coating forms over the MASN surface, consisting of a mixture of metallic and oxidized nickel (9 wt % Ni), and various species of boron (atomic ratio of Ni:B = 2). For unsupported NBC, metallic nickel nanocrystals (1−3 nm) were discovered imbedded within an amorphous matrix of a similar composition. Upon calcination at 550 °C in a N_2 atmosphere, partial conversion of unsupported NBC to crystalline Ni_3B was observed, whereas only crystalline metallic Ni was observed for NBC-MASN. To explain these differences, further evidence is given to suggest the presence of residual boron hydrides encapsulated in the bulk unsupported NBC, suggesting Ni_3B was an artifact of processing rather than an initial product.

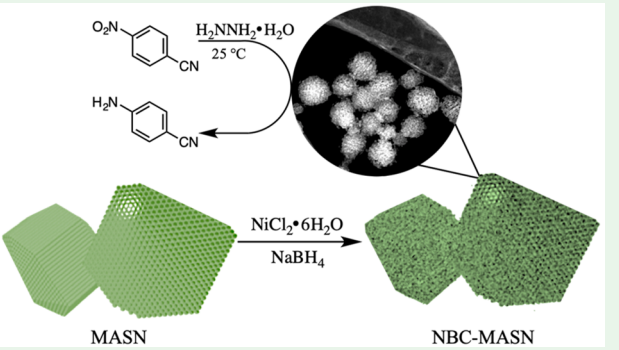

KEYWORDS: *nitroarene, catalysis, nickel, boron, hydrazine, borohydride, mesoporous silica*

INTRODUCTION

The reduction of nitroarenes to aromatic amines is of general interest for industrial as well as biological applications.[1] Traditionally, the synthesis of aromatic amines from their corresponding nitro compounds is performed at high temperatures and pressures, in the presence of hydrogen gas and a metallic catalyst such as Pt, Pd, Fe, Sn, or the well-known Raney nickel (eq 1).[2−4]

Arylnitro reduction by Raney Ni to arylamine products:[5]

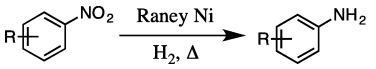

(1)

Alternatively, amorphous heterogeneous catalysts formed from reacting transition metal salts with sodium borohydride ($NaBH_4$) in protic solvents have a long history of success in a wide variety of reduction reaction schemes.[6−9] In aqueous media, sodium borohydride will generally reduce metal salts, such as $NiCl_2$ and $CoBr_2$, to their corresponding metallic (M^0) phase, while undergoing hydrolysis to form borate species and liberate hydrogen gas (eq 2).[10]

$$BH_4^- + 2M^{2+} + 2H_2O \rightarrow 2M + BO_2^- + 4H^+ + 2H_2 \quad (2)$$

The resulting black precipitates could be best described as nickel- or cobalt-based borate composites, both of which perform excellently in the catalytic hydrogenation of a variety of organic substrates containing reducible functional groups. Furthermore, the hydrolytic degradation of BH_4^- [11−13] and nickel-based composites is particularly successful at selectively reducing nitroarene compounds to their corresponding aniline derivatives.[14,15] However, the reusability of such catalysts is

Received: December 27, 2018
Accepted: February 8, 2019
Published: February 8, 2019

DOI: 10.1021/acsanm.8b02351
ACS Appl. Nano Mater. XXXX, XXX, XXX−XXX

Scheme 1. Schematic Illustration of (a) the Synthesis and (b) Use of NBC-MASN Catalyst for the Reduction of Nitroarenes with Hydrazine Hydrate

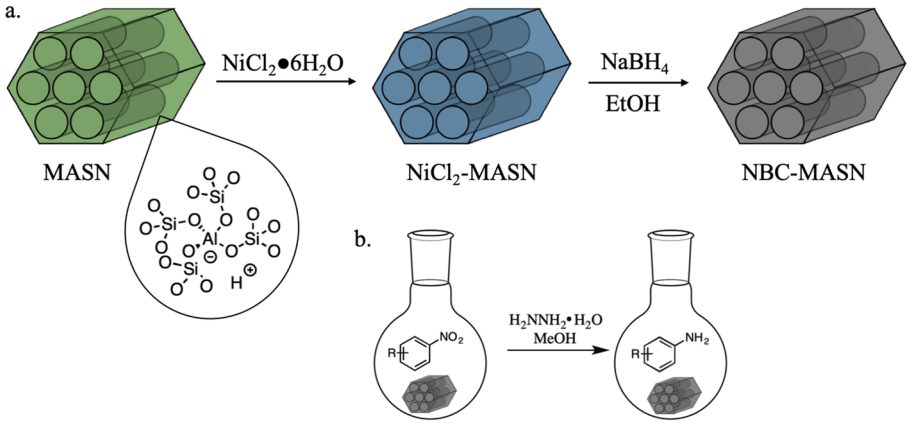

typically limited due to particle sintering, agglomeration, and surface oxidation. It has recently been shown that supporting these composites on inert scaffolds (such as titania, silica gel, organic polymers, or mesoporous silica nanoparticles) can enhance activity and reusability, compared to their bulk powders, by increasing catalyst surface area and stabilizing against particle agglomeration.[16−18] These catalysis schemes have also benefited from the use of safer and more stable chemical sources of hydrogen, such as hydrazine hydrate ($N_2H_4{\cdot}H_2O$).[14,16,19,20]

The motivation for our study was to investigate the safe and economically efficient reduction of nitroarenes, using $N_2H_4{\cdot}H_2O$ and a reusable amorphous nickel boron composite (NBC) catalyst supported on mesoporous aluminosilicate nanoparticles (MASN) (Scheme 1). In the course of this work, fundamental questions arose concerning the difference in physical character between supported and unsupported versions of NBC. These questions are discussed in light of considerable uncertainty in the literature as to the actual composition of such amorphous composites.[21−26]

In protic solvents at ambient pressure and temperature, most salts of the first row transition metals to the left of copper generate precipitates containing various boron species when reacted with excess $NaBH_4$, whereas copper and noble metal salts with more favorable reduction potentials tend to give pure metallic phases.[27] In the case of nickel (and similarly for cobalt), these precipitates have historically been termed amorphous nickel borides (Ni_3B, Ni_2B, etc.), a designation initially based on a combination of elemental analysis and powder X-ray diffraction studies of the crystalline structures which evolved upon heating in an inert atmosphere.[28−30] These amorphous precipitates are now known to be more structurally complex, possessing a variety of possible compositions and morphologies, depending on the choice of synthetic parameters (solvent system, pH, temperature, mixing rate, and the presence of oxygen in solution), the ratio of borohydride to nickel reacted, and the choice of nickel salt precursor.[27,31]

To explain the characteristically high activity of amorphous catalysts such as nickel−boron and cobalt−boron composites (NBC and CBC, respectively), earlier works in this field suggested the presence of a direct metal−boron interaction based on X-ray photoelectron spectroscopy (XPS) data. One scenario put forward is that electron donation occurs from boron to symmetry related transition metal d-orbitals and therefore increases catalytic activity through electron enrichment of the metal surface, while also sacrificially protecting the metal from oxidation.[31−38] However, a review of the previously published XPS data reveals a certain amount of ambiguity in assigning both the B 1s and Ni or Co 2p binding energy shifts to that of the corresponding borides as well as debate about the direction of electron donation between the metal and boron, in both the amorphous and crystalline compounds.[39]

With careful use of electron microscopy and elemental analysis, some authors have shown that bulk NBC and CBC powders are nanocomposites comprising single nanometer sized crystalline metal particles imbedded in an amorphous matrix containing boron oxides (transition or alkali metal borates, (poly)borates, etc.).[21−25,40] Although many of these authors invoke the presence of borides, they presume that the main function of the amorphous matrix is to physically prevent sintering and rapid oxidation of the catalytically active metal particles during synthesis, thereby preserving the large catalytic surface area claimed to be responsible for high activity.

While the exact nature of the metal−boron interaction in these amorphous materials remains uncertain, it is known that crystalline borides of transition metals are routinely formed under much more energetically demanding conditions than those of protic solvent synthesis at near-ambient conditions. Traditional nickel borides are synthesized in solid state reactions such as laser ablation or melt quenching of elemental Ni and B[41] or in nonprotic solvent systems at elevated temperatures (~90 °C).[27] Given that borohydrides are known to decompose readily in protic solvents[38] to produce $H_{2(g)}$ and various borates ($B(OH)_4^-$, BO_2^-, B_2O_3, polyborates, etc.), and given that this process is autocatalyzed in situ by the very same precipitates formed during the reaction of borohydrides with certain transition metal salts, particularly Ni^{2+} and Co^{2+},[12] it seems self-evident that protic solvent synthesis routes cannot produce true transition metal borides. It is much more plausible that such reactions primarily produce oxides of boron, which may then interact strongly with metallic precipitates to form amorphous transition metal and borate composites.[42] We are therefore careful not to label the bulk NBC and supported NBC-MASN catalysts studied in this work as a *nickel boride*, in recognition that the exact identities of the boron species present in such composites are still not entirely known.

Herein, we report the synthesis of an NBC-MASN catalyst for the efficient and selective reduction of arylnitro compounds

DOI: 10.1021/acsanm.8b02351
ACS Appl. Nano Mater. XXXX, XXX, XXX−XXX

to the corresponding arylamines using hydrazine hydrate as the hydrogen source. Additionally, NBC catalyst was examined to delineate the differences between supported and unsupported catalysts and to offer a preliminary explanation as to why the Ni_3B phase is only observed upon calcination of unsupported NBC in an inert atmosphere.

EXPERIMENTAL SECTION

All reagents were used as received without further purification. Milli-Q water (18.2 MΩ) was used throughout all steps of synthesis. High purity dry argon (Ar) was used during catalyst synthesis, storage, and use. 200 proof ethanol (EtOH) and hydrazine hydrate ($N_2H_4{\cdot}H_2O$) were purchased from Acros. Nickel chloride hexahydrate ($NiCl_2{\cdot}6H_2O$), sodium hydroxide (NaOH), aluminum isopropoxide (Al(O-*i*-Pr)$_3$), and sodium borohydride ($NaBH_4$) were purchased from Spectrum Laboratories. Cetyltrimethylammonium bromide (CTAB), tetraethoxysilane (TEOS), nitroarene substrates, and methanol (MeOH) were all purchased from Sigma-Aldrich.

Synthesis of MASN. Mesoporous aluminosilicate nanoparticles (MASN) were synthesized by adding a mixture of TEOS (4.58 g, 21.98 mmol) and Al(O-*i*-Pr)$_3$ (0.244 g, 1.19 mmol) (briefly sonicated) to a previously prepared solution consisting of water (485 g), CTAB (1.0 g, 2.74 mmol), and solid NaOH (2.80 g, 70.01 mmol). The CTAB and NaOH solution was first stirred for 15 min at 80 °C to homogenize, before adding the alkoxide mixture dropwise over 5 min. The combined solution was stirred at 80 °C for 2 h and then allowed to cool to room temperature while stirring for an additional hour. The cooled precipitate was filtered and washed with 1.0 L of Milli-Q water and then dried in vacuo overnight at 100 °C. The dried material was then ground to a fine powder and calcined in air at 550 °C for 5 h (at a heating rate of 1 °C/min) to remove the organic template.

Synthesis of NBC-MASN Catalyst. In a typical synthesis of NBC-MASN catalyst, MASN support (0.65 g) was dried in a vacuum oven overnight at 100 °C, cooled to room temperature, and then soaked in a solution of $NiCl_2{\cdot}6H_2O$ (0.26 g, 1.09 mmol) dissolved in 50/50 v/v EtOH and water. A minimal amount (∼3 mL) of solvent was used to create a thick slurry with the MASN. This slurry was sonicated in a tightly sealed 20 mL scintillation vial for 90 min and then allowed to soak for 5 days before drying overnight in a thoroughly $Ar_{(g)}$-purged vacuum oven at 100 °C. Dried $NiCl_2$-MASN was mechanically ground with $NaBH_4$ (0.084 g, 2.20 mmol) until thoroughly mixed together as a fine powder. The powder mixture was then gently purged with $Ar_{(g)}$ while cooling in a 0 °C water bath for 20 min, before rapidly introducing 19 mL of 0 °C absolute EtOH (200 proof) with vigorous magnetic stirring. The synthesis was performed in a semisealed scintillation vial with two small ports in the cap: one to allow for the introduction of a glass cannula into the reaction solution to deliver $Ar_{(g)}$ and the other for gas ventilation. The synthesis proceeded with continuous argon purging of the solution and rapid stirring for ∼2 h or until no more effervescent bubbling from $H_{2(g)}$ production could be observed. The solution was then diluted with 30 mL of room temperature water to help remove excess salts and centrifuged to isolate the solid, and the solid was dried overnight in an $Ar_{(g)}$-purged vacuum oven at 100 °C. The dry NBC-MASN catalyst was then stored under $Ar_{(g)}$ until use in catalysis or characterization.

Synthesis of NBC Catalyst. Unsupported, bulk NBC catalyst powder was synthesized by adding a solution of $NiCl_2{\cdot}6H_2O$ (0.26 g, 1.09 mmol) dissolved in 8.5 mL of absolute EtOH to a solution of $NaBH_4$ (0.084 g, 2.20 mmol) suspended in 8.5 mL of absolute EtOH, with rapid stirring at 0 °C under continuous $Ar_{(g)}$ purging as described above. Synthesis proceeded for ∼20 min or until no more $H_{2(g)}$ production could be observed, at which point the material was rinsed, retrieved, and dried as described above.

Calcination of As-Synthesized Catalysts. A custom-made calcination furnace with a quartz tube was used to heat the catalyst materials in either flowing nitrogen or air at 550 °C for 2 h at a heating rate of 10 °C min^{-1}.

General Procedure for the Reduction of Nitroarenes. To an argon-purged 50 mL round-bottom flask the NBC-MASN catalyst (0.235 g, 0.4 mmol of Ni), nitroarene (4 mmol), MeOH (8 mL), and either $N_2H_4{\cdot}H_2O$ (20 mmol) or a combination of $N_2H_4{\cdot}H_2O$ (20 mmol) and $NaBH_4$ (20 mmol) were added and allowed to stir at room temperature until no starting material was observed via ^{1}H NMR analysis. The reaction mixture was then centrifuged, and the supernatant decanted into a preweighed 100 mL round-bottom flask. The solid catalyst was rinsed with 15 mL of MeOH under brief sonication followed by centrifugation, and the supernatant was decanted into the same 100 mL flask. This rinse step was repeated, and the combined supernatants were then concentrated by rotary evaporation and analyzed via ^{1}H and ^{13}C NMR.

General Procedure for Cleaning NBC-MASN. The used NBC-MASN catalyst and methanol (2 × 15 mL) were combined in an argon-purged Falcon tube, the mixture was sonicated for 10 min and then centrifuged, and the supernatant was decanted. Ethanol (2 × 15 mL) was added to the catalyst, sonicated for 10 min, and centrifuged, and the supernatant was decanted. Methanol (10 mL) was added to the catalyst before sonication for 10 min and centrifuged, and the supernatant was decanted. The catalyst was then immediately reused.

General Procedure for the Regeneration of NBC-MASN. Cleaned (as above) and dried NBC-MASN and $NaBH_4$ (2 mol equiv of Ni, assuming Ni was 10 wt % of NBC-MASN) were added to an argon-purged Falcon tube capped with a rubber septum. The tube was cooled to 0 °C before adding 5 mL of 0 °C ethanol. The cold mixture was rapidly stirred for ∼1 h or until no more $H_{2(g)}$ production was observed. The mixture was then centrifuged, the supernatant decanted, and the recovered solid was rinsed as described above and dried in an argon-purged vacuum oven until further use.

Characterization. Powder X-ray diffraction (PXRD) was performed on a Rigaku SmartLab X-ray diffractometer with Cu Kα (1.54 Å) radiation (40 kV, 44 mA). All samples were prepared fresh and handled with minimal exposure to the atmosphere prior to scanning. All samples were ground under $Ar_{(g)}$ and evenly dispersed on an amorphous SiO_2 sample holder and scanned with a step size of 0.01° and scan rate of 1° min^{-1}. Annular dark field scanning transmission electron microscopy (ADF-STEM) imaging was performed on a FEI Titan TEM operated at 200 or 300 kV. The STEM probe had a convergence semiangle, α, of 10 mrad and a beam current of 25 pA (300 kV). HAADF-STEM images were acquired using a Fischione annular dark-field (ADF) detector. EDS data were simultaneously collected along with ADF-STEM data on four silicon drift detectors with a solid angle of 0.7 sr (SuperX) and analyzed using Bruker's Espirit software. HRTEM images were acquired using a FEI ThemIS microscope operated at 300 kV with a FEI Ceta camera. All electron microscopy and EDS data collection was performed on fresh samples suspended by brief sonication in absolute ethanol and deposited on 400 mesh copper TEM grids with lacey carbon support. Inductively coupled plasma optical emission spectroscopy (ICP-OES) data were collected on a PerkinElmer Optima 7000 DV. Samples for ICP-OES were prepared by digestion in an aqueous solution composed of 50 vol % concentrated HNO_3 and 5 vol % H_2O_2 (30% stock solution) at 85 °C, rapidly stirring in a sealed polypropylene container for 2 h prior to dilution with Milli-Q water. Thermogravimetric analysis (TGA) was performed on a TA Q500 thermoanalyzer, using a platinum weighing boat and flowing air during heating fresh samples at a rate of 10 °C min^{-1}. X-ray photoelectron spectroscopy was performed on a Kratos Axis Ultra spectrometer using an Al Kα source ($h\nu$ = 1486.69 eV) operated at 150 W and a hemispherical electron energy analyzer. Spectral positions were calibrated using adventitious alkyl carbon signals by shifting the C 1s peak to 284.8 eV. For samples which exhibited charging, a flood gun was used to neutralize the sample.

The products of catalysis reactions were analyzed by nuclear magnetic resonance (NMR) spectroscopy measured in ppm and recorded on a Bruker 500 MHz spectrometer at 297 K using $CDCl_3$ (δ = 7.26) as an internal standard for ^{1}H NMR and 125.7 MHz using $CDCl_3$ (δ = 77.0) as an internal standard for ^{13}C NMR. Using a different probe, ^{11}B NMR analysis occurred on a 160 MHz

DOI: 10.1021/acsanm.8b02351
ACS Appl. Nano Mater. XXXX, XXX, XXX−XXX

spectrometer using $BF_3{\cdot}Et_2O$ (δ = 0) as an external standard. Coupling constants (J) are given in hertz (Hz), and signal multiplicities are abbreviated as s = singlet, d = doublet, t = triplet, m = multiplet, and br = broad.

General Procedure for Hydrogen Evolution by Gas Buret. To the gas buret reservoir, outfitted with a rubber septum, 1 M HCl (15 mL), methanol (15 mL), and tetrahydrofuran (15 mL) were added and allowed to stir. A few trials of sacrificial hydride sources were used for the purpose of equilibrating the system. In a separate Ar-purged round-bottom flask, anhydrous $NiCl_2$ (0.065 g, 0.5 mmol) and solid $NaBH_4$ (0.038 g, 1 mmol) were added, and the flask was cooled to 0 °C. A cannula connected the round-bottom flask to the gas buret reservoir. The system was allowed to equilibrate before the addition of 4 mL of 0 °C ethanol via syringe. By the controlled relief of pressure in the closed system into a graduated cylinder, the volume of gas generated, plus total volume injected, was measured by water displacement. The temperature of the displaced water and barometric pressure were also measured as well as the temperature-dependent vapor pressure of water. The quantity of hydrogen produced was determined by following a previously published method.[43]

RESULTS AND DISCUSSION

We began this work by screening a number of catalysts made from different transition metal salts reacted with $NaBH_4$ in ethanol for the reduction of *p*-nitrotoluene to *p*-toluidine using hydrazine hydrate ($N_2H_4{\cdot}H_2O$) (Table S1). We found that $NiCl_2{\cdot}6H_2O$ was the most suitable precursor in forming a catalyst to this effect. The percent yield of *p*-toluidine was determined by isolation, and the purity was verified by ^{1}H NMR spectroscopy. We also found that supporting this catalyst, which we have termed nickel boron composite (NBC), on an inert scaffold made of mesoporous aluminosilicate nanoparticles (MASN) improved catalytic activity over the unsupported catalyst. The increased activity of the supported catalyst (NBC-MASN) was likely due to increased surface area of the active catalyst, as has been similarly demonstrated for cobalt−boron catalysts supported on mesoporous silica (MCM-41) nanoparticles.[44] MASN was chosen as a support because of the material's robust aluminosilicate structure, high surface area (~100 nm average diameter, ~1000 $m^2\ g^{-1}$), and mildly negative surface charge.[45] We hypothesized that these features would allow for good incorporation of Ni^{2+} into the support during impregnation with $NiCl_2{\cdot}6H_2O$ and also slow diffusion of Ni^{2+} out of MASN during reaction of dried $NiCl_2$-MASN with $NaBH_4$ in absolute ethanol. Attempts to support NBC on non-aluminated mesoporous silicate nanoparticles (MSN) resulted in a greater quantity of large, detached NBC particles formed separate from the MSN support, as observed by electron microscopy (Figure S1). The better retention and slowed diffusion of Ni^{2+} from MASN appear to allow for even distribution of the resulting composite material formed close to the MASN surface and possibly anchored within its mesochannels. Low-temperature (0 °C) synthesis was likewise chosen to allow for slower and more complete reaction of Ni^{2+} with BH_4^-. Indeed, the synthesis of NBC-MASN was found to take ~2 h to complete compared to ~20 min for the synthesis of unsupported NBC.

The initial catalysis reaction using fresh NBC-MASN in the reduction of *p*-nitrotoluene to *p*-toluidine reached completion after 2 h. Subsequent reuse cycles of the catalyst, however, showed progressively longer reaction periods to achieve full conversion of *p*-toluidine (Figure 1).

We speculated that the cause of the increasing reaction time required for complete conversion of *p*-nitrotoluene to *p*-toluidine might be due to a loss of catalytic surface area from the agglomeration of active Ni and/or passivation of the catalytic surface by NiO formation during successive catalyses. This prompted us to characterize the catalytic surface of NBC-MASN using various techniques. For structural comparison we included the characterization of unsupported NBC as well.

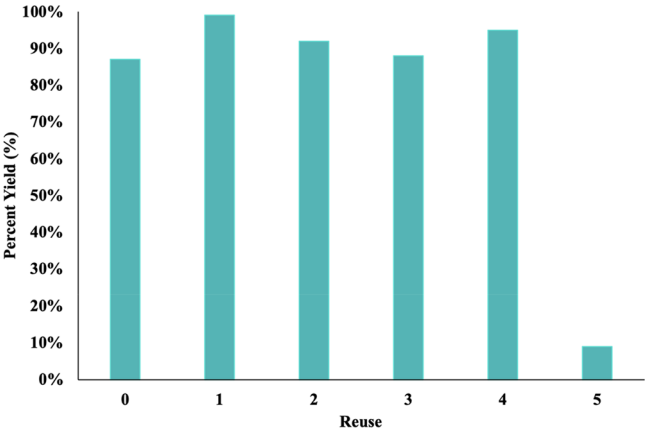

Figure 1. Percent yield of *p*-toluidine after successive reuse cycles of NBC-MASN. The yield was determined by isolation, and the purity was verified by ^{1}H NMR spectroscopy.

Annular dark field scanning transmission electron microscopy (ADF-STEM) imaging of NBC-MASN revealed a very thin (<10 nm) amorphous coating of material covering the honeycombed MASN particles (Figure 2a) after synthesis (Figure 2b). Synthesis of unsupported NBC typically gave particles in the hundreds of nanometers size regime (Figure 3a). Energy-dispersive X-ray spectroscopy (EDS) confirmed the presence of nickel in both NBC-MASN and unsupported NBC (Figure 3b), but detection of boron could not be confirmed due to its low signal intensity and overlap from the adjacent carbon signal (Figures S2 and S3). Given the more positive reduction potential of nickel, the majority of oxygen present in NBC (Figure 3c) is likely from borate species, rather than NiO, since freshly synthesized and carefully handled NBC should contain mostly reduced nickel. No information from EDS mapping of oxygen in NBC-MASN can be gained since the signal from SiO_2 overwhelms any contribution from borates.

Both ADF-STEM and high-resolution transmission electron microscopy (HRTEM) imaging of fresh NBC-MASN indicated the NBC coating was amorphous. If NBC-MASN particles were subjected to several minutes of continuous electron flux, however, it was observed that small spots of high contrast material developed on or within NBC-MASN (Figure 2c). EDS mapping revealed that these spots appear to correspond with higher concentrations of Ni compared to the bulk of the composite (Figure 2d). HRTEM shows these tiny regions have crystallinity (Figure 2 e,f), indicating the amorphous nickel in the composite segregated into larger particles and partially crystallized under the electron beam. The segregation/crystallization was particularly difficult to avoid during EDS mapping, wherein the samples were necessarily subjected to long exposures and higher beam current (Figure 2c,d). Figure S4 shows the progression of this segregation starting at 30 s and after 5 min. By comparison, HRTEM imaging of fresh unsupported NBC immediately revealed the presence of approximately 1−3 nm nanocrystalline domains of metallic Ni deposited within a surrounding

DOI: 10.1021/acsanm.8b02351
ACS Appl. Nano Mater. XXXX, XXX, XXX−XXX

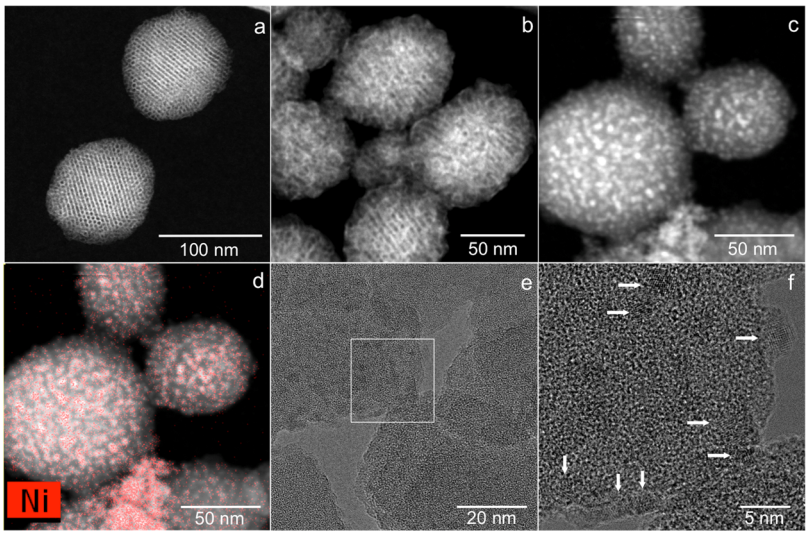

Figure 2. ADF-STEM images of (a) as-synthesized MASN, (b) NBC-MASN imaged within 30 s of beam exposure, and (c) NBC-MASN after EDS mapping for 5 min, with (d) the corresponding Ni EDS map. (e) HRTEM images of NBC-MASN after 5 min exposure to electron beam showing segregated regions of Ni and (f) a magnified section (box in panel e) showing lattice fringes associated with these regions (arrows).

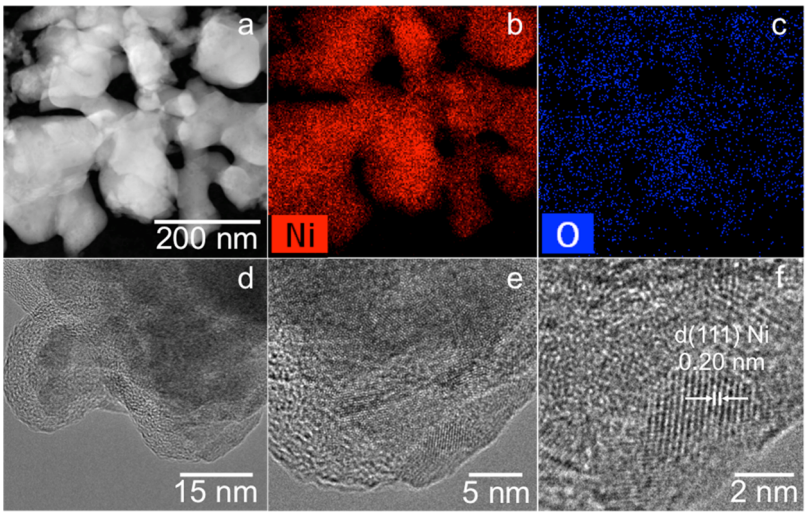

Figure 3. ADF-STEM image of (a) unsupported NBC, and corresponding EDS elemental maps of (b) Ni and (c) O present in the composite. HRTEM of unsupported NBC, imaged within 2 min of beam exposure, progressively magnified (d–f) to show lattice fringes for Ni nanocrystals embedded within an amorphous matrix.

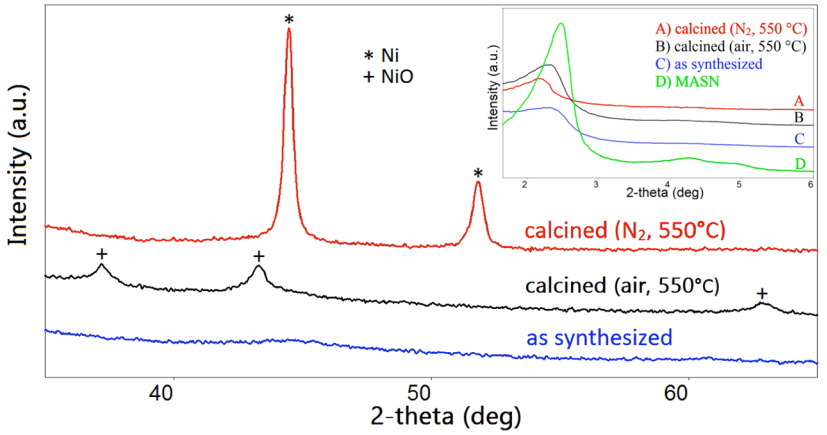

Figure 4. Comparison of PXRD profiles for as-synthesized (fresh) NBC-MASN and after calcination in air or flowing nitrogen. The inset shows the low angle diffraction pattern for the bare MASN compared to as-synthesized NBC-MASN before and after calcination.

DOI: 10.1021/acsanm.8b02351
ACS Appl. Nano Mater. XXXX, XXX, XXX−XXX

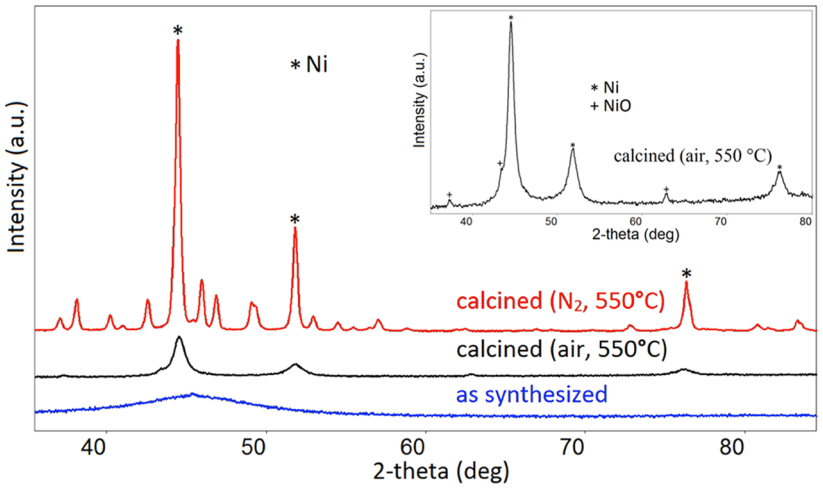

Figure 5. Comparison of PXRD profiles for as-synthesized (fresh) unsupported NBC and after calcination in air or flowing nitrogen. All peaks in the N_2-calcined sample not assigned to Ni (asterisks) can be assigned to Ni_3B (ICDD 00-048-1223). The inset shows an enlargement of the profile for the air-calcined material, indicating the presence of NiO.

amorphous matrix (Figure 3d−f and Figure S5), an observation consistent with previous reports of a similarly formed composite.[40] The unsupported NBC appeared much more stable under the electron beam than the amorphous surface of NBC-MASN, and additional segregation/crystallization of Ni was more difficult to observe during longer beam exposures in the case of unsupported NBC. This suggests that much of the metallic nickel resides as these preformed nanocrystals in unsupported NBC, whereas nickel in NBC-MASN is more homogeneously amorphous and evenly distributed within the NBC structure that coats the MASN.

As reported in the literature, heating these amorphous composites in inert atmospheres typically yields a mixture of crystalline nickel and nickel boride in bulk materials such as NBC.[28−30] Figures 4 and 5 show the powder X-ray diffraction (PXRD) profiles for NBC-MASN and NBC, respectively, in their as-synthesized (or fresh) form and after calcination in air or flowing nitrogen at 550 °C for 2 h. The high angle diffraction data for as-synthesized NBC-MASN display an amorphous profile, while that of unsupported NBC gives only a broad peak occurring near the (111) reflection for fcc Ni (44.5° 2θ). This lack of appreciable diffraction from the nanocrystalline nickel present in fresh unsupported NBC can be explained by their small size, below the ∼5 nm domain cutoff necessary to produce X-ray diffraction in metallic nanoparticles.[46,47] Calcining NBC and NBC-MASN in either air or $N_{2(g)}$ gave crystalline diffraction profiles in both cases, likely due in part to the same segregation/crystallization phenomena observed by electron microscopy. Interestingly, the air-calcined NBC-MASN diffraction profile shows only peaks indexed to NiO, whereas the unsupported NBC calcined in air gave a profile showing predominantly metallic Ni, with relatively low intensity peaks for NiO. The $N_{2(g)}$-calcined NBC-MASN gave a profile for metallic Ni, whereas similar calcination of unsupported NBC yielded a mixture of crystalline Ni and Ni_3B (ICDD 00-048-1223).

In an attempt to explain this commonly reported formation of Ni_3B upon calcination of NBC in an inert atmosphere, we offer preliminary evidence to suggest there may be residual boron hydrides within the amorphous matrix of NBC. It has been previously shown that various alkali earth and transition metal borohydrides and boranes [$Mg(BH_4)$, $Ti(BH_4)_3$, $Zr(BH_4)_4$, $Hf(BH_4)_4$, and $Cr(B_3H_8)_2$] can undergo thermal decomposition to form the corresponding metal borides at moderately high temperatures (>400 °C).[48−53] In particular, it has been shown that Ni_3B can be formed at 530 °C from the precursors $NiCl_2$ and various boranes (B_5H_9 or $B_{10}H_{14}$).[54] Thermal decomposition of residual boron hydrides during calcination of NBC would explain why crystalline nickel boride phases were observed in NBC catalyst (eq 3).

$$NiCl_2 + 2NaBH_4 \rightarrow Ni(BH_4)_2 + NaCl \xrightarrow{\Delta} \text{“}Ni_2B\text{”} \xrightarrow{Ni^0} Ni_3B \quad (3)$$

It should be pointed out that if unsupported NBC is first refluxed in MeOH for several hours prior to $N_{2(g)}$ calcination, then only crystalline Ni is observed (Figure S6). Refluxing in methanol has been previously shown to remove residual boron hydrides from similar materials,[8] which we presume become trapped in the composite during the rapid reaction of Ni^{2+} and BH_4^-. ^{11}B NMR analysis of the supernatant solution of the refluxed material provided a singlet at 18 ppm, suggesting that a borate is formed from hydrolysis of borohydride (Figure S7). Trapped boron hydride [possibly $Ni(BH_4)_2$][27] or hydrogen adducts[55] in the matrix of unsupported NBC may then decompose during heating, explaining the formation of Ni_3B upon $N_{2(g)}$ calcination (eq 3) as well as the predominance of Ni over NiO upon air calcination of unsupported NBC. The slow formation of the thin NBC layer in NBC-MASN may prevent this entrapment of boron hydrides and would explain the formation of both Ni upon $N_{2(g)}$ calcination and NiO upon air calcination of NBC-MASN.

The predominance of Ni compared to NiO in the PXRD profile of air-calcined NBC may also be attributed to the sintering and surface passivation of the Ni nanocrystals during heating. These agglomerated Ni nanocrystals may retain interior particle domains of Ni sufficiently large to diffract X-rays, while being protected from further oxidation by an exterior layer composed of NiO and borate, as previously shown for similarly formed cobalt boron composites.[21] In the case of air-calcined NBC-MASN, where only NiO is present in the PXRD profile, it may be that the very thin layer of homogeneously amorphous NBC coating of the MASN is more extensively oxidized than in bulk unsupported NBC. Finally, in the case of $N_{2(g)}$ calcination of NBC-MASN,

DOI: 10.1021/acsanm.8b02351
ACS Appl. Nano Mater. XXXX, XXX, XXX−XXX

amorphous Ni present in the NBC-MASN simply segregates and crystallizes in domains large enough to diffract X-rays.

Calcining NBC or NBC-MASN in either air or $N_{2(g)}$ atmosphere diminished the catalytic activity toward the reduction of aromatic nitro groups, likely due to nickel segregation/crystallization and a subsequent loss of catalytic surface area, as well as catalytically inactive surface NiO in the case of air calcination.

The location of NBC on the external surface of MASN is apparent in Figure 2, but whether this material extends into the mesochannels of the support is less apparent due to the low contrast between NBC and SiO_2. Some information can be determined, however, from low angle PXRD of the material. The inset in Figure 4 shows the change in the (100) peak position and intensity for the MASN support, before and after NBC formation and subsequent calcination in air or nitrogen. This peak corresponds to the distance between the walls of the ∼3 nm diameter channels that run through the MASN spheres. The reduction of intensity and slight shift to lower 2θ angles may be attributed respectively to inclusion of NBC material within the channels and a subtle expansion of the pores as a result of their partial degradation during calcination.[40] This degradation is not typically seen upon template extraction during MASN synthesis, which occurs at the same temperature of 550 °C, so it may result here in part from the growth of a crystalline nickel phase within the mesochannels upon calcination of NBC-MASN. Inclusion of the NBC coating within the channels of MASN may indicate that the composite is partially anchored in the pores of the MASN, allowing it to remain highly dispersed and catalytically active over multiple reuse cycles (vide infra).

Thermogravimetric analysis (TGA) of both unsupported NBC and NBC-MASN was performed to investigate the possible decomposition of trapped borohydride in NBC in general as well as the oxidation of metallic nickel in both materials (Figure S8). Upon heating to 800 °C in air, NBC-MASN shows only the expected mass loss associated with removal of physically adsorbed water, with no appreciable mass gain that would indicate oxidation of boron or nickel. Considering that PXRD clearly shows the formation of NiO at 550 °C in air-calcined NBC-MASN, this TGA result is not easily explained. However, a similar TGA of unsupported NBC demonstrated two increases in mass initiating at approximately 350 and 650 °C. The first mass gain initiates very close to that observed for $NaBH_4$ similarly heated in air, which initiates at a temperature of ∼360 °C, and may indicate the presence of residual borohydride in unsupported NBC, while the second mass increase starting at ∼650 °C is consistent with the oxidation of Ni nanoparticles in the nanometer size regime.[56]

Because the surface of a catalytic material is of particular interest, X-ray photoelectron spectroscopy (XPS) was used in an attempt to identify the surface species present in both NBC-MASN and unsupported NBC. Figures S9 and S10 show the wide scans and core-level scans for freshly prepared samples of both NBC-MASN and NBC, respectively. Table 1 gives the relevant electron binding energies for Ni, B, and O in each material. It is evident from the Ni 2p core-level scans that the catalyst surface in both cases contains a mixture of metallic and oxidized nickel. The B 1s core-level scans show the presence of oxidized boron as well as a peak occurring at 187.7 eV for both materials, which is within the region typically assigned to nickel boride in the literature.[31−33] The interpretation of this B 1s peak and its assignment to nickel boride is difficult to make,

Table 1. Binding Energies of NBC-MASN and NBC

element	NBC-MASN (eV)	NBC (eV)	possible compounds
Ni 2p	852.6	852.3	Ni
	856.8	856.6	NiO, $Ni(OH)_2$, $Ni(BO_2)_2$
B 1s	187.7	187.7	B_xH_y
	193.0	192.4	BO_2^-, B_2O_3
O 1s	532.8	532.3	NiO, BO_2^-, B_2O_3

considering the very slight shifts in binding energy observed between elemental boron, borohydride, and the relevant borides.[39] As for the B 1s shifts in these materials, the assigned shifts for Ni 2p binding energies are also typically <1 eV from that of metallic Ni.[31,33,57] There is also considerable and longstanding disagreement as to whether electron donation occurs from boron to metal, or vice versa, in amorphous nickel borides.[39] Evidence has been given of residual hydrides or hydrogen adducts in both nickel and cobalt composites, particularly when synthesized in ethanol, though the specific identity of these purported hydrides (M−H or B−H) has not been resolved.[55] Considering the interpretation of PXRD and TGA data in this work, we reason that the B 1s binding energy previously reported by others as evidence of amorphous nickel boride may actually be indicative of residual borohydride sequestered in the composite upon formation. Indeed, the presence of residual borohydride in similar nickel-based composites has been previously reported.[8] Upon comparison of the spectra for NBC-MASN and unsupported NBC, the greatly diminished intensity of this B 1s peak at 187.7 eV relative to the adjacent borate peak implies a much lower surface concentration of this boron species in NBC-MASN. Considering the NBC layer on MASN appears by ADF-STEM to be quite thin (perhaps only a few nanometers on average), the XPS analysis, with a reliable surface penetration depth of 5−10 nm, may largely account for the entire composition of the NBC layer in NBC-MASN. Assuming the B 1s peak at 187.7 eV arises from sequestered borohydride, then its lower concentration in NBC-MASN could account for the lack of any Ni_3B phase observed by PXRD after calcining in $N_{2(g)}$. Of course, some portion of the initial $NaBH_4$ will fully react and become borate in the composite matrix (or rinse away as boric acid), which explains why a mixture of metallic nickel and nickel boride is typically seen after calcination of NBC in $N_{2(g)}$.

Further evidence for the presence of borohydride trapped within the matrix of NBC was given by examining the quantity of hydrogen evolved during synthesis of both unsupported and supported NBC (Table S2). For unsupported NBC, only 51% of the theoretical amount of hydrogen was released when $NiCl_2$:$NaBH_4$ (1:2) was allowed to react at 0 °C in ethanol. Even when varying the ratio of $NiCl_2$:$NaBH_4$ from 1:1 to 1:0.5, the amount of hydrogen evolved was 43% and 54%, respectively. Similar results were obtained for $NiCl_2$-MASN:$NaBH_4$ (1:2), which liberated 56% of the theoretical amount of hydrogen, indicating that some B−H compound remains unreacted, possibly sequestered within the interstitial spaces of the material.

The bulk nickel and boron content in both NBC-MASN and unsupported NBC were determined by inductively coupled plasma optical emission spectroscopy (ICP-OES). Throughout this work, the content of Ni initially present in fresh NBC-MASN averaged 9.0 wt %, while the calculated loading of Ni^{2+} into MASN via impregnation with $NiCl_2{\cdot}6H_2O$ was 10 wt %. However, no significant amount of Ni was observed by ICP-

DOI: 10.1021/acsanm.8b02351
ACS Appl. Nano Mater. XXXX, XXX, XXX−XXX

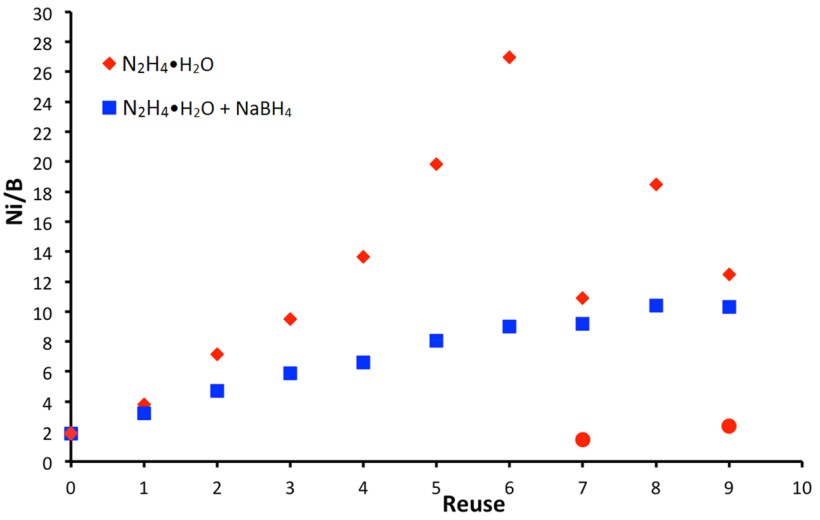

Figure 6. ICP-OES data for the Ni:B molar ratio in NBC-MASN after successive reuses in the catalytic hydrogenation of *p*-nitrotoluene. Two reaction conditions are compared: $N_2H_4{\cdot}H_2O$ as reducing agent (red diamonds) and $N_2H_4{\cdot}H_2O$ with an equimolar addition of $NaBH_4$ (blue squares). The two red circular markers for reuse numbers 7 and 9 indicate the Ni:B ratio after ex situ regeneration of NBC-MASN with $NaBH_4$ but before catalysis using $N_2H_4{\cdot}H_2O$.

OES in the ethanol/water supernatant collected after the syntheses of either NBC or NBC-MASN. Therefore, additional moisture adsorbed in the hydrated nickel salt and instrumental error inherent during ICP-OES may account for the discrepancy. The initial ratio of Ni:B was ~2 in both NBC and NBC-MASN and remained unchanged for both catalysts after calcination in either nitrogen or air.

ICP-OES was further used to track changes in the nickel and boron content after successive reuses of NBC-MASN in the reduction of *p*-nitrotoluene to *p*-toluidine. Figures 6 and 7

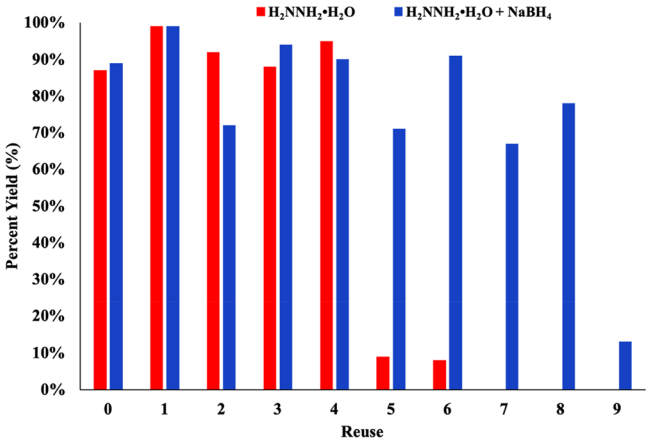

Figure 7. Reuse study: the percent yield for the conversion of *p*-nitrotoluene to *p*-toluidine is plotted against reuse cycle number, using either $N_2H_4{\cdot}H_2O$ as the reducing agent or a combination of $N_2H_4{\cdot}H_2O$ and $NaBH_4$ as reducing and regenerating agents. The product yields were determined after 24 h reaction. The yield was determined by isolation, and the purity was verified by ^{1}H NMR spectroscopy.

show respectively the Ni:B ratio NBC-MASN and the percent yield of *p*-toluidine determined after 24 h by ^{1}H NMR for two different reuse studies. In both studies, 5 mmol of $N_2H_4{\cdot}H_2O$ was used as the reducing agent for 1 mmol of *p*-nitrotoluene, in the presence of NBC-MASN containing ~0.1 mmol of nickel. Sodium borohydride was used either ex situ or in situ with $N_2H_4{\cdot}H_2O$, in an attempt to prolong the catalyst's reusable lifetime. In the ex situ $NaBH_4$ study, when the percent yield of *p*-toluidine was observed to decrease significantly (below 80%) upon cycling, the used NBC-MASN catalyst was cleaned, dried (see the Experimental Section), and regeneration attempted by reacting it with a quantity of $NaBH_4$ equivalent to twice the molar amount of Ni assumed to be present in the catalyst. In the in situ $NaBH_4$ reuse study, a combination of $N_2H_4{\cdot}H_2O$ and equimolar $NaBH_4$ was used, with the intention of affecting continuous in situ regeneration of the catalyst by reaction with $NaBH_4$. As can be seen in Figure 6, a progressive loss of boron from NBC-MASN is observed upon each cycle in both studies but is more dramatic in the study where only $N_2H_4{\cdot}H_2O$ is present, compared to in situ regeneration by $NaBH_4$. As can be seen in Figure 7, the use of $NaBH_4$ along with $N_2H_4{\cdot}H_2O$ extends the lifetime of the catalyst up to nine reuse cycles compared to only four cycles when regeneration is performed ex situ. No significant loss of nickel from NBC-MASN was observed during either reuse study, indicating that all of the Ni^{2+} initially loaded onto MASN was reacted during the synthesis of the catalyst.

It must be pointed out that $N_2H_4{\cdot}H_2O$ will not reduce NiO to Ni^0 at 25 °C, and oxidation from continuous reaction with the substrate nitro group during catalysis makes oxidation of the catalyst inevitable.[58] The sustained catalytic activity of NBC-MASN observed when both $NaBH_4$ and $N_2H_4{\cdot}H_2O$ were present during each catalysis cycle (Figure 7) is attributed to the ability of borohydride to reduce passivating surface NiO. It is also possible, given the higher average boron content compared to the ex situ study, that in situ $NaBH_4$ may replenish some protective borate species that physically prevent agglomeration of the active nickel or its more rapid oxidation. In contrast, it was found that exposing the catalyst to additional borohydride ex situ, as soon as catalytic activity was observed to decrease, did not improve catalytic performance upon subsequent reuse. As can be seen in Figure 6, the boron content in NBC-MASN did increase after these ex situ borohydride treatments prior to reuse 7 and 9 but sharply decreased again upon further cycling. We interpret this as evidence that $NaBH_4$ is reducing oxides formed on the

DOI: 10.1021/acsanm.8b02351
ACS Appl. Nano Mater. XXXX, XXX, XXX−XXX

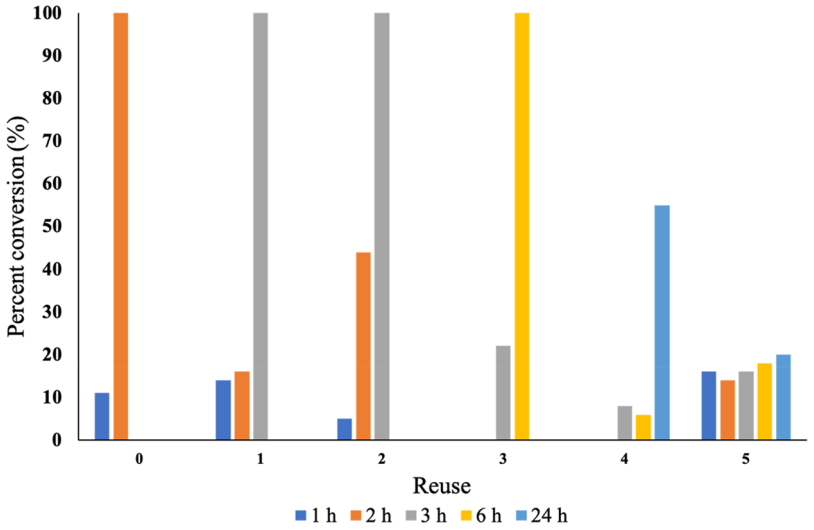

Figure 8. Percent conversion of *p*-nitrotoluene as determined by ^{1}H NMR analysis.

catalytically active nickel surface, so long as the oxidation is not too extensive—as may be the case in the ex situ regeneration study. Severe oxidation of the amorphous nickel, along with loss of the surrounding borate matrix, may leave the nickel constituent vulnerable to agglomeration, and loss of surface area, during subsequent reduction by borohydride. Further XPS and electron microscopy studies examining the surface oxidation and agglomeration/crystallization of nickel at each reuse cycle would likely elucidate the point at which surface oxidation and/or segregation/crystallization deactivates the catalyst, and either in situ or ex situ borohydride regeneration is no longer possible for NBC-MASN.

A ^{1}H NMR spectroscopic study was performed to determine at what time the nitroarene was converted into the aniline derivative (Figure 8). Fresh NBC-MASN catalyst completely converted *p*-nitrotoluene to *p*-toluidine in 2 h (reuse 0). However, subsequent reuses of the catalyst showed progressively longer reaction times to achieve full conversion of *p*-toluidine. The longer reaction time required is evidence of the formation of an oxide layer on the catalytic nickel surface, which inhibits hydrazine and the nitroarene from interacting with the catalyst as effectively when compared to the freshly made NBC-MASN.[4] Although full conversion to *p*-toluidine was not achieved in the fifth cycle, all of the starting material was consumed, leaving behind a mixture of *p*-toluidine and several intermediates (Figure S11).

A possible reaction pathway (Figure S12) can be elucidated based on the types of intermediates present in the ^{1}H NMR. The presence of 4,4-dimethylazoxybenzene and 4,4-dimethylhydrazobenzene suggests that the reduction of *p*-nitrotoluene begins with the reduction of the nitro group to a nitroso intermediate (Figure S12, A). The nitroso intermediate then condenses with a molecule of the hydroxylamine (B) to generate the 4,4-dimethylazoxybenzene intermediate (C), which leads to the 4,4-dimethylhydrazobenzene (E) intermediate and last the desired *p*-toluidine.[14,59−63]

To verify the catalytic ability of NBC-MASN for the reduction of other nitroarenes, a preliminary substrate scope was investigated (Table 2). Simple nitroarenes such as *p*-nitrotoluene and nitrobenzene easily produced the aniline products (entries 1 and 2). Halogenated nitroarenes were reduced in excellent yields to the corresponding aniline derivatives, and no dehalogenated product was observed (entry 3). Both trisubstituted and pyrene nitroarene derivatives were tolerated as well (entries 4 and 5).

Table 2. NBC-MASN versus NBC for Selective Nitro Group Reduction

Entry	Substrate	Product	Catalyst[a]	
			NBC-MASN[b]	NBC[c]
1	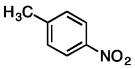	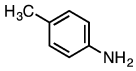	94%	85%
2			99%	58%
3	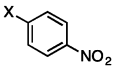 X = Br, Cl, I	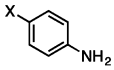 X = Br, Cl, I	99% X = Br, Cl, I	X = Br 83% X = Cl 96% X = I 87%
4	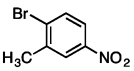	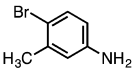	99%	99%
5	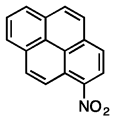	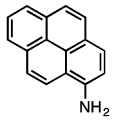	99%	89%
6	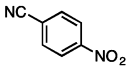	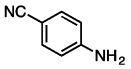	48%	19%
7	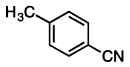	--	0%	--

[a]Isolated yield. [b]Reaction conditions for supported catalyst: nitroarene (4 mmol), NBC-MASN (10 mol %), MeOH (8 mL), hydrazine hydrate (20 mmol), 25 °C, 24 h, under an argon atmosphere. [c]Reaction conditions for unsupported catalyst: nitroarene (4 mmol), NBC (10 mol %), MeOH (8 mL), hydrazine hydrate (20 mmol), 25 °C, 24 h, under an argon atmosphere.

Interestingly, 4-nitrobenzonitrile was selectively reduced to 4-cyanobenzylamine (entry 6) while the nitrile in 4-cyanotoluene remained unreacted during the catalysis (entry 7). This selectivity differs from previously published catalyst systems, which reduced both nitro and nitrile groups simultaneously.[5,64,65] In those methodologies, the reducing

DOI: 10.1021/acsanm.8b02351
ACS Appl. Nano Mater. XXXX, XXX, XXX−XXX

agent was H_2 generated from $NaBH_4$, while our catalysis system uses $N_2H_4{\cdot}H_2O$. This result confirms that the reducing agent can dictate functional group selectivity.[60] Thus, the formation of a diimide, from the oxidation of hydrazine,[66−69] reacts preferentially with the nitro substituent before decomposing into nontoxic $N_{2(g)}$.

Overall, the initial arylamine product yield was higher for a variety of substrates when using supported NBC-MASN catalyst compared with the unsupported NBC catalyst. This is likely due to the more amorphous character of NBC grown on MASN, potentially possessing a larger proportion of minimally coordinated nickel sites for catalysis, compared to the more crystalline character of NBC.[70,71] Similar arguments have been made for the enhanced activity of Co−B when dispersed on mesoporous silica nanoparticles (MSN) versus solid silica beads or bulk Co−B, where larger domains of metallic Co tend to aggregate.[44]

CONCLUSIONS

In this work, we have shown that a nickel boron composite (NBC) supported on mesoporous aluminosilicate nanoparticles (NBC-MASN) increases catalytic activity compared to unsupported NBC for the selective reduction of several different nitroarenes to their corresponding aniline derivatives. The catalytically active amorphous nickel in NBC-MASN may be deactivated by oxidation and/or agglomeration/crystallization of nickel during catalysis, leading to an average reusable lifetime of four cycles. The reusable lifetime of the catalyst could be prolonged up to nine cycles (for the reduction of *p*-nitrotoluene) when equimolar $NaBH_4$ was used with $N_2H_4{\cdot}H_2O$ during catalysis, but not when $NaBH_4$ was used ex situ to attempt regeneration of the exhausted catalyst. Introducing $NaBH_4$ in situ during catalysis likely reduces surface NiO back to Ni and may help to fortify the borate content believed responsible for preventing agglomeration and rapid oxidation of the amorphous nickel present in NBC.

The structural character and negative surface charge of the MASN support appears to aid in forming a thin, highly dispersed amorphous coating of NBC on MASN during synthesis. Comparatively, unsupported NBC consists of much larger particles containing 1−3 nm metallic nickel nanocrystals embedded in an amorphous matrix. We attribute the boron content in NBC-MASN, observed by ICP-OES and XPS, largely to the presence of unknown borate species rather than amorphous nickel boride, since the degradation of borohydrides in protic solvents prohibits the formation of elemental boron or true borides. The XPS, TGA, and PXRD analyses, along with the results of methanol refluxing, indicate the possible entrapment of borohydrides within the rapidly formed precipitate of unsupported NBC. This residual borohydride may explain the formation of Ni_3B upon $N_{2(g)}$ calcining of unsupported NBC. The slower formation of the thin NBC layer grown on MASN may allow for a more complete reaction of $NaBH_4$ and would explain why only crystalline Ni is observed by PXRD upon $N_{2(g)}$ calcining of NBC-MASN as well as the greatly reduced intensity of the B 1s peak at 187.7 eV in the case of NBC-MASN compared to that of unsupported NBC. The same 2:1 Ni:B ratio observed by ICP-OES for both NBC-MASN and unsupported NBC may be explained if the majority of boron present in the supported catalyst is oxidized, while some portion of the boron in NBC is residual boron hydride trapped within the amorphous matrix. We have given preliminary evidence indicating the presence of residual boron hydrides in unsupported NBC.

ASSOCIATED CONTENT

Supporting Information

The Supporting Information is available free of charge on the ACS Publications website at DOI: 10.1021/acsanm.8b02351.

Further details on the experimental methods, physical characterization, and results (PDF)

AUTHOR INFORMATION

Corresponding Authors

*E-mail: singaram@ucsc.edu.

*E-mail: soliver@ucsc.edu.

ORCID

Jason Cooper: 0000-0002-7953-4229

Bakthan Singaram: 0000-0002-3986-6528

Scott R. J. Oliver: 0000-0002-6160-1518

Author Contributions

J.L.H. and G.A. contributed equally.

Notes

The authors declare no competing financial interest.

ACKNOWLEDGMENTS

This work was partially supported by funds from The Ima Hernandez Foundation and the National Science Foundation (Grant 1603754). Work at the Molecular Foundry was supported by the Office of Science, Office of Basic Energy Sciences, of the U.S. Department of Energy under Contract DE-AC02-05CH11231.

REFERENCES

(1) Vogt, P. F.; Gerulis, J. J. Amines, Aromatic. In *Ullmann's Encyclopedia of Industrial Chemistry*; Wiley-VCH Verlag GmbH & Co. KGaA: Weinheim, Germany, 2000; pp 699−718.

(2) Booth, G. Nitro Compounds, Aromatic. In *Ullmann's Encyclopedia of Industrial Chemistry*; Wiley-VCH Verlag GmbH & Co. KGaA: Weinheim, Germany, 2000; pp 301−349.

(3) Wehner, V.; Jäger, V. Synthesis OfD- AndL-2-Amino-2-Deoxyarabinose and 1,4-Dideoxy-1,4-Iminolyxitol by (C2+ C3)-Nitroaldol Addition with 2-O-Benzylglyceraldehyde. *Angew. Chem., Int. Ed. Engl.* **1990**, *29*, 1169−1171.

(4) Petkar, D. R.; Kadu, B. S.; Chikate, R. C. Highly Efficient and Chemoselective Transfer Hydrogenation of Nitroarenes at Room Temperature over Magnetically Separable Fe−Ni Bimetallic Nanoparticles. *RSC Adv.* **2014**, *4*, 8004−8010.

(5) Schreifels, J. A.; Maybury, P. C.; Swartz, W. E. Comparison of the Activity and Lifetime of Raney Nickel and Nickel Boride in the Hydrogenation of Various Functional Groups. *J. Org. Chem.* **1981**, *46*, 1263−1269.

(6) Brown, C. A.; Ahuja, V. K. Catalytic Hydrogenation. VI. The Reaction of Sodium Borohydride with Nickel Salts in Ethanol Solution. P-2 Nickel, A Highly Convenient, New, Selective Hydrogenation Catalyst with Great Sensitivity to Substrate Structure. *J. Org. Chem.* **1973**, *38*, 2226−2230.

(7) Paul, R.; Buisson, P.; Joseph, N. Catalytic Activity of Nickel Borides. *Ind. Eng. Chem.* **1952**, *44*, 1006−1010.

(8) Belisle, C. M.; Young, Y. M.; Singaram, B. Catalytic Reaction. 1. Catalytic 1,4-Hydrogenation of α,β-Unsaturated Aldehydes and Ketones Using SC-1 Nickel Boride. *Tetrahedron Lett.* **1994**, *35*, 5595−5598.

(9) Leggans, E. K.; Barker, T. J.; Duncan, K. K.; Boger, D. L. Iron(III)/$NaBH_4$-Mediated Additions to Unactivated Alkenes: Syn-

DOI: 10.1021/acsanm.8b02351
ACS Appl. Nano Mater. XXXX, XXX, XXX−XXX

thesis of Novel 20′-Vinblastine Analogues. *Org. Lett.* **2012**, *14*, 1428−1431.
(10) Schaefer, Z. L.; Ke, X.; Schiffer, P.; Schaak, R. E. Direct Solution Synthesis, Reaction Pathway Studies, and Structural Characterization of Crystalline Ni_3B Nanoparticles. *J. Phys. Chem. C* **2008**, *112*, 19846−19851.
(11) Wade, R. C.; Holah, D. G.; Hughes, A. N.; Hui, B. C. Catalytically Active Borohydride-Reduced Nickel and Cobalt Systems. *Catal. Rev.: Sci. Eng.* **1976**, *14*, 211−246.
(12) Schlesinger, H. I.; Brown, H. C.; Finholt, A. E.; Gilbreath, J. R.; Hoekstra, H. R.; Hyde, E. K. Sodium Borohydride, Its Hydrolysis and Its Use as a Reducing Agent and in the Generation of Hydrogen[1]. *J. Am. Chem. Soc.* **1953**, *75*, 215−219.
(13) Khurana, J. M.; Gogia, A. Synthetically Useful Reactions with Nickel Boride A Review. *Org. Prep. Proced. Int.* **1997**, *29*, 1−32.
(14) Zhang, J.; Lu, G.; Cai, C. Chemoselective Transfer Hydrogenation of Nitroarenes by Highly Dispersed Ni-Co BMNPs. *Catal. Commun.* **2016**, *84*, 25−29.
(15) Nose, A.; Kudo, T. Reduction with Sodium Borohydride-Transition Metal Salt Systems. I. Reduction of Aromatic Nitro Compounds with the Sodium Borohydride-Nickelous Chloride System. *Chem. Pharm. Bull.* **1981**, *29*, 1159−1161.
(16) Rahman, A.; Jonnalagadda, S. B. Swift and Selective Reduction of Nitroaromatics to Aromatic Amines with Ni−Boride−Silica Catalysts System at Low Temperature. *Catal. Lett.* **2008**, *123*, 264−268.
(17) Wong, S.-T.; Lee, J.-F.; Chen, J.-M.; Mou, C.-Y. Preparation and Characterization of MCM-41 and Silica Supported Nickel Boride Catalysts. *J. Mol. Catal. A: Chem.* **2001**, *165*, 159−167.
(18) Yang, X.; Sun, J.-K.; Kitta, M.; Pang, H.; Xu, Q. Encapsulating Highly Catalytically Active Metal Nanoclusters inside Porous Organic Cages. *Nat. Catal.* **2018**, *1*, 214−220.
(19) Rai, R. K.; Mahata, A.; Mukhopadhyay, S.; Gupta, S.; Li, P.-Z.; Nguyen, K. T.; Zhao, Y.; Pathak, B.; Singh, S. K. Room-Temperature Chemoselective Reduction of Nitro Groups Using Non-Noble Metal Nanocatalysts in Water. *Inorg. Chem.* **2014**, *53*, 2904−2909.
(20) Prathap, K. J.; Wu, Q.; Olsson, R. T.; Dinér, P. Catalytic Reductions and Tandem Reactions of Nitro Compounds Using in Situ Prepared Nickel Boride Catalyst in Nanocellulose Solution. *Org. Lett.* **2017**, *19*, 4746−4749.
(21) Arzac, G. M.; Rojas, T. C.; Fernández, A. Boron Compounds as Stabilizers of a Complex Microstructure in a Co-B-Based Catalyst for $NaBH_4$ Hydrolysis. *ChemCatChem* **2011**, *3*, 1305−1313.
(22) Cavaliere, S.; Hannauer, J.; Demirci, U. B.; Akdim, O.; Miele, P. Ex Situ Characterization of $N_2H_4^-$, $NaBH_4$- and NH_3BH_3-Reduced Cobalt Catalysts Used in $NaBH_4$ Hydrolysis. *Catal. Today* **2011**, *170*, 3−12.
(23) Kalidindi, S. B.; Vernekar, A. A.; Jagirdar, B. R. Co−Co_2B, Ni−Ni_3B and Co−Ni−B Nanocomposites Catalyzed Ammonia−Borane Methanolysis for Hydrogen Generation. *Phys. Chem. Chem. Phys.* **2009**, *11*, 770−775.
(24) Demirci, U. B.; Miele, P. Cobalt-Based Catalysts for the Hydrolysis of $NaBH_4$ and NH_3BH_3. *Phys. Chem. Chem. Phys.* **2014**, *16*, 6872−6885.
(25) Ozerova, A. M.; Bulavchenko, O. A.; Komova, O. V.; Netskina, O. V.; Zaikovskii, V. I.; Odegova, G. V.; Simagina, V. I. Cobalt Boride Catalysts for Hydrogen Storage Systems Based on NH_3BH_3 and $NaBH_4$. *Kinet. Catal.* **2012**, *53*, 511−520.
(26) Geng, J.; Jefferson, D. A.; Johnson, B. F. G. Exploring the Structural Complexities of Metal-Metalloid Nanoparticles: The Case of Ni·B as Catalyst. *Chem. - Eur. J.* **2009**, *15*, 1134−1143.
(27) Glavee, G. N.; Klabunde, K. J.; Sorensen, C. M.; Hadjipanayis, G. C. Borohydride Reduction of Nickel and Copper Ions in Aqueous and Nonaqueous Media. Controllable Chemistry Leading to Nanoscale Metal and Metal Boride Particles. *Langmuir* **1994**, *10*, 4726−4730.
(28) Hofer, L. J. E.; Shultz, J. F.; Panson, R. D.; Anderson, R. B. The Nature of the Nickel Boride Formed by the Action of Sodium Borohydride on Nickel Salts. *Inorg. Chem.* **1964**, *3*, 1783−1785.
(29) He, Y.; Qiao, M.; Hu, H.; Pei, Y.; Li, H.; Deng, J.; Fan, K. Preparation of Amorphous Ni−B Alloy: The Effect of Feeding Order, Precursor Salt, pH and Adding Rate. *Mater. Lett.* **2002**, *56*, 952−957.
(30) Corrias, A.; Ennas, G.; Licheri, G.; Marongiu, G.; Paschina, G. Amorphous Metallic Powders Prepared by Chemical Reduction of Metal Ions with Potassium Borohydride in Aqueous Solution. *Chem. Mater.* **1990**, *2*, 363−366.
(31) Okamoto, Y.; Nitta, Y.; Imanaka, T.; Teranishi, S. Surface Characterization of Nickel Boride and Nickel Phosphide Catalysts by X-Ray Photoelectron Spectroscopy. *J. Chem. Soc., Faraday Trans. 1* **1979**, *75*, 2027−2039.
(32) Legrand, J.; Gota, S.; Guittet, M.-J.; Petit, C. Synthesis and XPS Characterization of Nickel Boride Nanoparticles. *Langmuir* **2002**, *18*, 4131−4137.
(33) Schreifels, J. X-Ray Photoelectron Spectroscopy of Nickel Boride Catalysts: Correlation of Surface States with Reaction Products in the Hydrogenation of Acrylonitrile. *J. Catal.* **1980**, *65*, 195−206.
(34) Yoshida, S.; Yamashita, H.; Funabiki, T.; Yonezawa, T. Catalysis by Amorphous Metal Alloys. Part 1.—Hydrogenation of Olefins over Amorphous Ni−P and Ni−B Alloys. *J. Chem. Soc., Faraday Trans. 1* **1984**, *80*, 1435−1446.
(35) Deng, J.; et al. The Study of Ultrafine Ni-B and Ni-P Amorphous Alloy Powders as Catalysts. *J. Catal.* **1994**, *150*, 434−438.
(36) Li, H. Liquid Phase Hydrogenation of Acetonitrile to Ethylamine over the Co_B Amorphous Alloy Catalyst. *J. Catal.* **2003**, *214*, 15−25.
(37) Fernandes, R.; Patel, N.; Miotello, A.; Filippi, M. Studies on Catalytic Behavior of Co−Ni−B in Hydrogen Production by Hydrolysis of $NaBH_4$. *J. Mol. Catal. A: Chem.* **2009**, *298*, 1−6.
(38) Liu, Y.-C.; Huang, C.-Y.; Chen, Y.-W. Hydrogenation of P-Chloronitrobenzene on Ni−B Nanometal Catalysts. *J. Nanopart. Res.* **2006**, *8*, 223−234.
(39) Carenco, S.; Portehault, D.; Boissière, C.; Mézailles, N.; Sanchez, C. Nanoscaled Metal Borides and Phosphides: Recent Developments and Perspectives. *Chem. Rev.* **2013**, *113*, 7981−8065.
(40) Geng, J.; Jefferson, D. A.; Johnson, B. F. G. The Unusual Nanostructure of Nickel−Boron Catalyst. *Chem. Commun.* **2007**, No. 9, 969−971.
(41) Akopov, G.; Yeung, M. T.; Kaner, R. B. Rediscovering the Crystal Chemistry of Borides. *Adv. Mater.* **2017**, *29*, 1604506−1604535.
(42) Prasanth, C. P.; Ebbin, J.; Abhijith, A.; Nair, D. S.; Ibnusaud, I.; Raskatov, J.; Singaram, B. Stabilization of $NaBH_4$ in Methanol Using a Catalytic Amount of NaOMe. Reduction of Esters and Lactones at Room Temperature without Solvent-Induced Loss of Hydride. *J. Org. Chem.* **2018**, *83*, 1431−1440.
(43) Clary, J. W.; Rettenmaier, T. J.; Snelling, R.; Bryks, W.; Banwell, J.; Wipke, W. T.; Singaram, B. Hydride as a Leaving Group in the Reaction of Pinacolborane with Halides under Ambient Grignard and Barbier Conditions. One-Pot Synthesis of Alkyl, Aryl, Heteroaryl, Vinyl, and Allyl Pinacolboronic Esters. *J. Org. Chem.* **2011**, *76*, 9602−9610.
(44) Patel, N.; Fernandes, R.; Edla, R.; Lihitkar, P. B.; Kothari, D. C.; Miotello, A. Superior Hydrogen Production Rate by Catalytic Hydrolysis of Ammonia Borane Using Co-B Nanoparticles Supported Over Mesoporous Silica Particles. *Catal. Commun.* **2012**, *23*, 39−42.
(45) Hauser, J. L.; Tran, D. T.; Conley, E. T.; Saunders, J. M.; Bustillo, K. C.; Oliver, S. R. J. Plasma Treatment of Silver Impregnated Mesoporous Aluminosilicate Nanoparticles for Adsorptive Desulfurization. *Chem. Mater.* **2016**, *28*, 474−479.
(46) Kondrat, S. A.; Shaw, G.; Freakley, S. J.; He, Q.; Hampton, J.; Edwards, J. K.; Miedziak, P. J.; Davies, T. E.; Carley, A. F.; Taylor, S. H.; Kiely, C. J.; Hutchings, G. J. Physical Mixing of Metal Acetates: A Simple, Scalable Method to Produce Active Chloride Free Bimetallic Catalysts. *Chem. Sci.* **2012**, *3*, 2965−2971.
(47) Yan, W.; Chen, B.; Mahurin, S. M.; Schwartz, V.; Mullins, D. R.; Lupini, A. R.; Pennycook, S. J.; Dai, S.; Overbury, S. H. Preparation and Comparison of Supported Gold Nanocatalysts on

DOI: 10.1021/acsanm.8b02351
ACS Appl. Nano Mater. XXXX, XXX, XXX−XXX

Anatase, Brookite, Rutile, and P25 Polymorphs of TiO_2 for Catalytic Oxidation of CO. *J. Phys. Chem. B* **2005**, *109*, 10676−10685.
(48) Saldan, I. Decomposition and Formation of Magnesium Borohydride. *Int. J. Hydrogen Energy* **2016**, *41*, 11201−11224.
(49) Crociani, L.; Rossetto, G.; Kaciulis, S.; Mezzi, A.; El-Habra, N.; Palmieri, V. Study of Magnesium Boride Films Obtained from $Mg(BH_4)_2$ by CVD. *Chem. Vap. Deposition* **2007**, *13*, 414−419.
(50) Jensen, J. A.; Gozum, J. E.; Pollina, D. M.; Girolami, G. S. Titanium, Zirconium, and Hafnium Tetrahydroborates as "Tailored" CVD Precursors for Metal Diboride Thin Films. *J. Am. Chem. Soc.* **1988**, *110*, 1643−1644.
(51) Jayaraman, S.; Yang, Y.; Kim, D. Y.; Girolami, G. S.; Abelson, J. R. Hafnium Diboride Thin Films by Chemical Vapor Deposition from a Single Source Precursor. *J. Vac. Sci. Technol., A* **2005**, *23*, 1619−1625.
(52) Rice, G. W.; Woodin, R. L. Zirconium Borohydride as a Zirconium Boride Precursor. *J. Am. Ceram. Soc.* **1988**, *71*, C-181−C−183.
(53) Goedde, D. M.; Girolami, G. S. A New Class of CVD Precursors to Metal Borides: $Cr(B_3H_8)_2$ and Related Octahydrotriborate Complexes. *J. Am. Chem. Soc.* **2004**, *126*, 12230−12231.
(54) Kher, S. S.; Spencer, J. T. Chemical Vapor Deposition Precursor Chemistry. 3. Formation and Characterization of Crystalline Nickel Boride Thin Films from the Cluster-Assisted Deposition of Polyhedral Borane Compounds. *Chem. Mater.* **1992**, *4*, 538−544.
(55) Maybury, P. C.; Mitchell, R. W.; Hawthorne, M. F. Hydrogen Adducts of Cobalt and Nickel Boride. *J. Chem. Soc., Chem. Commun.* **1974**, *0*, 534−535.
(56) Beygi, H.; Sajjadi, S. A. Magnetic Properties of Crystalline Nickel and Low Phosphorus Amorphous Ni 1-X P x Nanoparticles. *Mater. Chem. Phys.* **2018**, *204*, 403−409.
(57) Hendrickson, D. N.; Hollander, J. M.; Jolly, W. L. Core-Electron Binding Energies for Compounds of Boron, Carbon, and Chromium. *Inorg. Chem.* **1970**, *9*, 612−615.
(58) Chekin, F.; Sadeghi, S. Room Temperature Decomposition of Hydrazine Catalyzed by Nickel Oxide Nanoparticles. *Bulgarian Chem. Commun.* **2015**, *47*, 714−719.
(59) Pogorelić, I.; Filipan-Litvić, M.; Merkaš, S.; Ljubić, G.; Cepanec, I.; Litvić, M. Rapid, Efficient and Selective Reduction of Aromatic Nitro Compounds with Sodium Borohydride and Raney Nickel. *J. Mol. Catal. A: Chem.* **2007**, *274*, 202−207.
(60) Vernekar, A. A.; Patil, S.; Bhat, C.; Tilve, S. G. Magnetically Recoverable Catalytic Co−Co_2B Nanocomposites for the Chemoselective Reduction of Aromatic Nitro Compounds. *RSC Adv.* **2013**, *3*, 13243−13250.
(61) Gabriel, C. M.; Parmentier, M.; Riegert, C.; Lanz, M.; Handa, S.; Lipshutz, B. H.; Gallou, F. Sustainable and Scalable Fe/Ppm Pd Nanoparticle Nitro Group Reductions in Water at Room Temperature. *Org. Process Res. Dev.* **2017**, *21*, 247−252.
(62) Moore, R. E.; Furst, A. Reductions with Hydrazine Hydrate Catalyzed by Raney Nickel. 111. Effect of the Catalyst on the Reduction of 2,2'-Dinitrobiphenyl. *J. Org. Chem.* **1958**, *23*, 1504−1506.
(63) Corma, A.; Concepción, P.; Serna, P. A Different Reaction Pathway for the Reduction of Aromatic Nitro Compounds on Gold Catalysts. *Angew. Chem., Int. Ed.* **2007**, *46*, 7266−7269.
(64) Caddick, S.; Judd, D. B.; Lewis, A. K. d. K.; Reich, M. T.; Williams, M. R. A Generic Approach for the Catalytic Reduction of Nitriles. *Tetrahedron* **2003**, *59*, 5417−5423.
(65) Osby, J. O.; Heinzman, S. W.; Ganem, B. Studies on the Mechanism of Transition-Metal-Assisted Sodium Borohydride and Lithium Aluminum Hydride Reductions. *J. Am. Chem. Soc.* **1986**, *108*, 67−72.
(66) Cantillo, D.; Moghaddam, M. M.; Kappe, C. O. Hydrazine-Mediated Reduction of Nitro and Azide Functionalities Catalyzed by Highly Active and Reusable Magnetic Iron Oxide Nanocrystals. *J. Org. Chem.* **2013**, *78*, 4530−4542.
(67) Larsen, J. W.; Freund, M.; Kim, K. Y.; Sidovar, M.; Stuart, J. L. Mechanism of the Carbon Catalyzed Reduction of Nitrobenzene by Hydrazine. *Carbon* **2000**, *38*, 655−661.
(68) Kumarraja, M. Simple and Efficient Reduction of Nitroarenes by Hydrazine in Faujasite Zeolites. *Appl. Catal., A* **2004**, *265*, 135−139.
(69) Zhao, Z.; Yang, H.; Li, Y.; Guo, X. Cobalt-Modified Molybdenum Carbide as an Efficient Catalyst for Chemoselective Reduction of Aromatic Nitro Compounds. *Green Chem.* **2014**, *16*, 1274−1281.
(70) Prathap, K. J.; Wu, Q.; Olsson, R. T.; Dinér, P. Catalytic Reductions and Tandem Reactions of Nitro Compounds Using in Situ Prepared Nickel Boride Catalyst in Nanocellulose Solution. *Org. Lett.* **2017**, *19*, 4746−4749.
(71) Zhang, J.; Cai, Y.; Lu, G.; Cai, C. Facile and Selective Hydrogenolysis of β-O-4 Linkages in Lignin Catalyzed by Pd−Ni Bimetallic Nanoparticles Supported on ZrO_2. *Green Chem.* **2016**, *18*, 6229−6235.

DOI: 10.1021/acsanm.8b02351
ACS Appl. Nano Mater. XXXX, XXX, XXX−XXX